

---

---

DIFFRACTION AND SCATTERING  
OF IONIZING RADIATIONS

---

---

## Experimental Study of the Method of X-ray Phase-Contrast Microscopy Using a Nanofocusing Lens at KISI-Kurchatov Synchrotron Source

M. S. Folomeshkin<sup>a,\*</sup>, V. G. Kohn<sup>a</sup>, A. Yu. Seregin<sup>a</sup>, Yu. A. Volkovsky<sup>a</sup>, P. A. Prosekov<sup>a</sup>, V. A. Yunkin<sup>b</sup>,  
A. A. Snigirev<sup>c</sup>, Yu. V. Pisarevsky<sup>a</sup>, A. E. Blagov<sup>a</sup>, and M. V. Kovalchuk<sup>a</sup>

<sup>a</sup>National Research Centre “Kurchatov Institute,” Moscow, 123182 Russia

<sup>b</sup>Institute of Microelectronics Technology and High Purity Materials, Russian Academy of Sciences,  
Chernogolovka, Moscow oblast, 142432 Russia

<sup>c</sup>Immanuel Kant Baltic Federal University, Kaliningrad, 236016 Russia

\*e-mail: folmaxim@gmail.com

Received September 20, 2024; revised September 20, 2024; accepted September 24, 2024

**Abstract**—The results of the experimental study at the KISI-Kurchatov synchrotron source of the new phase-contrast imaging scheme for micro-objects using a nanofocusing compound refractive lens are presented. Visualization with submicron spatial resolution of a Fresnel zone plate with the width of the outer zones less than 0.5  $\mu\text{m}$  is demonstrated. It is found that in the performed experiments the main contribution to the instrumental function, which limits the spatial resolution, is due to the vibrations of the optical scheme elements. The possibility of using the proposed scheme for estimating the beam transverse size at the focus of the compound refractive lens, with allowance for the instrumental function, is demonstrated.

DOI: 10.1134/S1063774524602429

### INTRODUCTION

The creation of the third-generation synchrotron radiation (SR) sources in the end of the last century stimulated active development of the methods of coherent X-ray microscopy for studying the structure of organic and inorganic micro-objects. The development of such methods of study appears to be especially urgent in Russia in view of the development of fourth-generation SR sources [1] for structural analysis with a nanoscale spatial resolution [2]. The simplest and most widespread method is X-ray phase-contrast microscopy [3].

The advantages of near-field phase-contrast microscopy over other methods for visualizing micro-objects are the absence of strict requirements to the spatial coherence of the SR beam and the possibility of direct observation of the characteristic features of the micro-object studied (size, period, etc.). However, when studying relatively small micro-objects (less than 10  $\mu\text{m}$  in size), this method meets a problem related to the insufficiently high resolution of modern area detectors for recording images of this size. This problem can be overcome using nanofocusing X-ray optics, which forms a secondary SR source before the sample studied. The SR beam, diverging after the secondary source, provides a geometric magnification of

the image, with conservation of the near-field diffraction condition.

A scheme of phase-contrast microscopy was proposed and theoretically considered in [4]; in this scheme, the secondary SR source is formed using a nanofocusing compound refractive lens (NCRL) [5, 6]. A numerical experiment on imaging a photonic crystal structure showed that this scheme makes it possible to visualize a structure with a period less than 0.5  $\mu\text{m}$ .

In this paper, we report the results of the first experimental study of this scheme by an example of imaging the structure of a Fresnel zone plate (FZP) with a width of outer zones less than 0.5  $\mu\text{m}$ . The KISI-Kurchatov synchrotron radiation source was used. It was found that NCRLs can successfully be used even with a source having a relatively low degree of spatial coherence when applying a method that does not require a high spatial coherence. Experimentally recorded phase-contrast images made it possible to determine the FZP structure period in the region of outer zones with a submicron accuracy. An analysis of the obtained experimental data showed that it is the vibrations of the optical scheme elements rather than the finite spatial coherence of the SR beam that most greatly deteriorate the spatial resolution.

## THEORETICAL BASES

We will briefly consider the theory of coherent X-ray optics. The scalar wave field of monochromatic SR with energy  $E$ , propagating along the optical axis  $z$ , is presented in the form of the product of a slowly varying function and a rapidly varying exponential:

$$\Psi(x, z) = \exp(ikz)\psi(x, z), \quad (1)$$

where  $k = 2\pi/\lambda$  is the wavenumber,  $\lambda = hc/E$  is the radiation wavelength,  $h$  is Planck's constant, and  $c$  is the speed of light in vacuum. The measurable in the experiment is the SR intensity, and it is sufficient to be limited to the consideration of only the slowly varying function  $\psi(x, z)$ . The quantity  $\psi(x, z)$  will be referred below as the SR wave function (WF).

The WF transfer along  $z$  over empty space from  $z_0$  to  $z_1$  is described in correspondence with the Huygens–Fresnel principle:

$$\psi(x, z_1) = P(x, z_1 - z_0) * \psi(x, z_0), \quad (2)$$

where  $P(x, z) = (i\lambda z)^{-1/2} \exp(i\pi x^2/\lambda z)$  is the Fresnel propagator. The symbol  $*$  denotes the convolution operation.

The change in the WF when passing through a fairly thin micro-object can be described in the projection approximation using multiplication by the transmission function

$$T(x) = \exp(ik[n - 1]t(x)), \quad (3)$$

where  $n$  is the complex refractive index of SR in the micro-object material and  $t(x)$  is micro-object thickness along the  $z$  axis.

On SR sources, it is individual electrons that emit in a bending magnet or undulator. Each electron emits a spherical wave in the intrinsic coordinate system; however, because of the relativistic effects, the radiation beam has a small angular divergence during propagation along the  $z$  axis. Individual electrons emit spontaneously at different times and, therefore, incoherently. This fact determines the specific way of taking into account the transverse source size  $w_s$ . It is necessary to calculate the radiation intensity on the detector from each point and then to sum the intensity from all points. For a point SR source with a coordinate  $x_s$ , located at a distance  $z_s$  from the micro-object studied, the WF on the detector, located at a distance  $z_d$  after micro-object, is described, in correspondence with (2) and (3), by the expression

$$\Psi_d(x, x_s) = P(x, z_d) * T(x)P(x - x_s, z_s). \quad (4)$$

The distance  $z_s$  is generally several tens of meters; therefore, the WF incident on the sample studied can approximately be considered as a plane wave if the source size  $w_s$  is sufficiently small. In this case,

$$\Psi_d(x) = P(x, z_d) * T(x). \quad (5)$$

It follows from the theory that the intensity distribution  $I_d(x) = |\Psi_d(x)|^2$  depends on three parameters: radiation wavelength  $\lambda$ , micro-object size  $D$ , and the distance  $z_d$  at which the image is recorded. This dependence is expressed in terms of the diameter of the first Fresnel zone  $D_f = 2(\lambda z)^{1/2}$ . The near-field diffraction region corresponds to the condition  $D \gg D_f$ , at which intensity contrast arises at the micro-object edges.

The near-field region is used in phase-contrast microscopy [3, 7] for direct observation of the boundaries of objects studied. However, when passing to the study of micro-objects, there arises a problem related to the fact that the image size in the near field is approximately equal to the micro-object size. The resolution of modern area detectors ( $\sim 0.5 \mu\text{m}$ ) is insufficient for recording images of this size. In addition, the distance at which the near-field condition is implemented may be less than 1 mm for micro-objects, which also hinders performance of experiments.

The aforementioned problems can be solved with the aid of nanofocusing X-ray optics, which is used to form a secondary SR source before the sample studied. This optics provides geometric magnification of the recorded image, as can be shown by transforming (4) in the following way:

$$\begin{aligned} \Psi_d(x, x_s) P^{-1}(x - x_s, z_t) \\ = P(x_e + x_s z_d/z_t, z_e) * T(x_e), \end{aligned} \quad (6)$$

where  $z_t = z_s + z_d$ ,  $x_e = x/M$ ,  $z_e = z_d/M$ ,  $M = z_t/z_s$ . The parameter  $M$  is the factor of geometric magnification of sizes on the detector in comparison with the sizes on the object. The Fresnel propagator in the left-hand side of (6) does not affect the shape of the intensity profile and only scales the image intensity in correspondence with the energy conservation law. The right-hand side of (6) for  $x_s = 0$  is equivalent to (5), but for other scale  $x_e$  and diminished distance to the detector,  $z_e$ . A displacement of a point SR source in the direction perpendicular to the optical axis leads to displacement of image as a whole by  $-x_s z_d/z_s$ . Thus, locating the point SR source sufficiently close to the micro-object studied, one can increase significantly the phase-contrast image size with conservation of the near-field condition for the effective distance  $z_e$ .

A scheme was theoretically considered in [4], where the secondary SR source is formed using a planar NCRL (Fig. 1a). Planar NCRLs, fabricated using the technology of deep anisotropic etching of silicon [5, 6], belong to the most promising SR nanofocusing tools. The developed technology of deep anisotropic etching of silicon makes it possible to form precisely NCRLs with an aperture of  $50 \mu\text{m}$  or less (Figs. 1b, 1c). The refracting surface of these NCRLs is a parabolic cylinder, which provides linear focusing of a coherent beam to a transverse size less than  $50 \text{ nm}$  [8]. NCRLs consist of many individual elements, which are characterized by the following set of param-

eters: aperture  $A$ ; refracting surface curvature radius  $R$ ; minimum thickness  $d$ ; and element length along the optical axis,  $p = d + A^2/4R$ . Note that relatively long NCRLs, the focal length of which is comparable with their geometric length, cannot be considered in the projection approximation; therefore, other approaches must be used to calculate the focused beam in this case. The theory of SR focusing using NCRLs was developed in [9–13]. Theoretical consideration was performed for both strongly absorbing NCRLs [9–11], for which the influence of the aperture of elements can be neglected, and weakly absorbing ones [12, 13], for which the finite aperture affects the focusing result. To calculate the wave function after an NCRL for the aforementioned cases, one can use, for example, the universal XRWP program [14], designed for carrying out calculations in the field of coherent X-ray optics. In addition, there is an on-line program [15], which allows one to calculate the focused beam parameters [11].

It follows from the theory of strongly absorbing NCRLs that the wave function of radiation after an NCRL is a Gaussian beam, characterized by an angular divergence  $\Delta\theta$  and focal FWHM (full width at half maximum)  $w_f$ . These parameters are interrelated in the following way:

$$w_f = (2 \ln 2 / \pi) (\lambda / \Delta\theta) = 0.441 (\lambda / \Delta\theta). \quad (7)$$

It is known that, for a Gaussian beam at a distance  $z \gg z_R$  from the focus, where  $z_R = (\pi/2 \ln 2) (w_f/\lambda) = 2.27 (w_f/\lambda)$  is the Rayleigh length, the transverse dependence of the WF phase is parabolic; i.e., it corresponds to the radiation from a point source in the paraxial approximation. Thus, the Gaussian beam after an NCRL can be used, similarly to a point source, to magnify the image. The only difference is that the intensity of this beam has a finite angular divergence. The angular divergence of the beam must be taken into account to ensure complete illumination of the micro-object or its region under study. For example, for the radiation energy  $E = 18$  keV and beam size in the focus  $w_f = 50$  nm, the angular divergence is  $\Delta\theta = 606$   $\mu\text{rad}$ . The Rayleigh length is  $z_R = 82$   $\mu\text{m}$  in this case. At the distance  $z = 100 z_R$  from the NCRL focus, the SR beam FWHM is 5  $\mu\text{m}$ , which quite sufficient to illuminate micro-objects.

Note also that the SR beam nanofocusing using NCRL can be implemented only using coherent radiation. For an extended SR source, the beam in the NCRL focus is a diminished source image, whose size exceeds the focal size for coherent radiation. The size of the SR source image can be determined within the theory of NCRL focusing, in particular, using the on-line-program [15]. Thus, the resolution of the phase-contrast scheme with a secondary source is determined by the incoherent beam size in the NCRL focus.

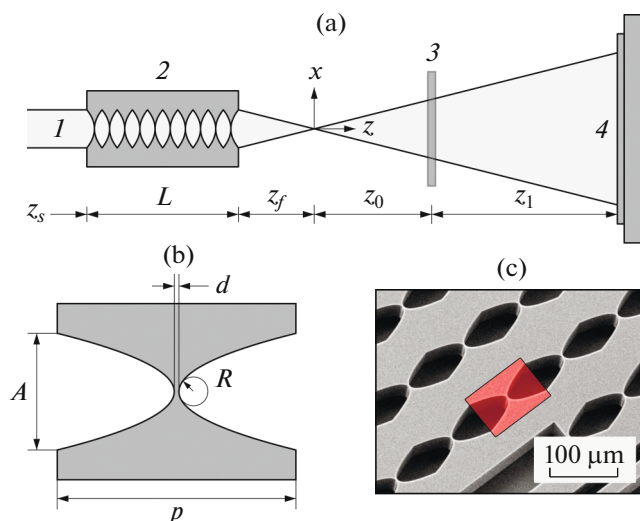


**Fig. 1.** (a) Scheme of phase-contrast microscopy using a planar NCRL: (1) monochromatic SR beam, (2) NCRL, (3) micro-object, and (4) detector. (b) Schematic image of an NCRL element. (c) SEM image of a planar NCRL on a silicon surface (the NCRL element is framed).

## EXPERIMENTAL DETAILS

The experimental study of the method of X-ray phase-contrast microscopy using NCRL (Fig. 1a) was performed on the XCPM (X-ray Crystallography and Physical Materials Science) beamline of the KISI-Kurchatov synchrotron source.

A photograph of the experimental scheme is presented in Fig. 2a. The SR source on the XCPM beamline is a bending magnet, located at a distance  $z_s = 15$  m from the sample. The size of the SR source formed by the bending magnet is well approximated by a two-dimensional Gaussian function with FWHM of  $\sim 100 \times 1000$   $\mu\text{m}^2$  in the vertical and horizontal directions, respectively. The angular divergence of the SR beam is approximately  $100 \times 1000$   $\mu\text{rad}^2$  in the corresponding planes. A more detailed technical description of the beamline can be found in [16].

The SR beam was monochromatized using a double-crystal Si(111) monochromator, whose angular position was tuned to the photon energy  $E = 18$  keV. The monochromator provided a relative spectral resolution  $\Delta E/E \sim 10^{-4}$ . To suppress higher harmonics with energies multiple of the ground harmonic energy  $E$ , the second monochromator crystal was detuned from the exact Bragg position by approximately 10  $\mu\text{rad}$ . With this tuning, the ground harmonic intensity was  $\sim 80\%$  of the maximum value.

The SR beam focusing (aimed at forming a secondary source) was performed using an integral silicon chip with one-dimensional focusing NCRLs of different length (with different numbers of elements) and the following parameters of elements (Fig. 1b):  $A = 50$   $\mu\text{m}$ ,  $R = 6.25$   $\mu\text{m}$ ,  $d = 2$   $\mu\text{m}$ , and  $p = 102$   $\mu\text{m}$ .

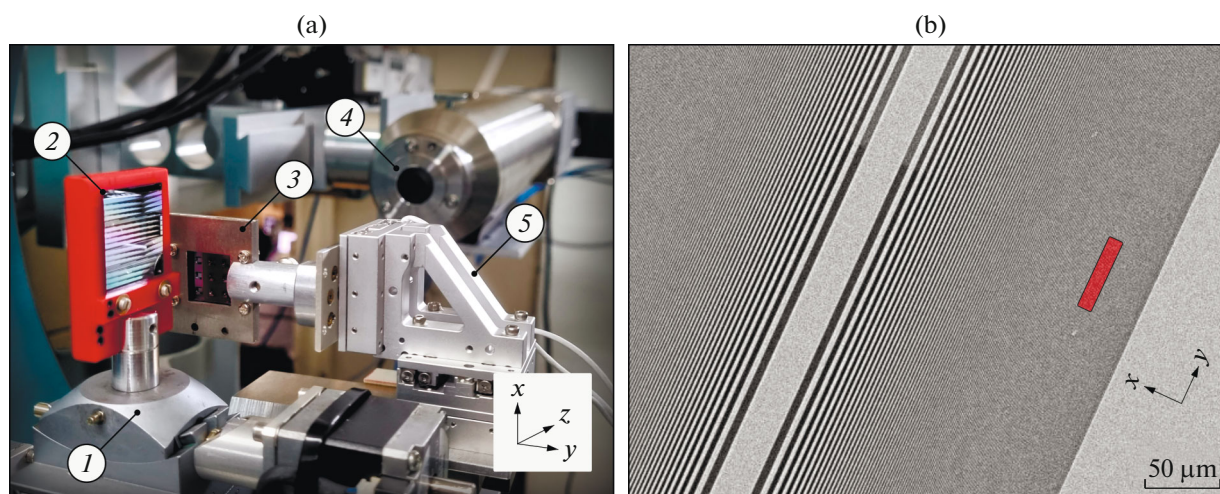


**Fig. 2.** (a) Photograph of experimental scheme elements: (1) five-circle goniometer, (2) silicon chip with NCRL, (3) frame holder with FZP, (4) area detector, and (5) piezo drivers. (b) SEM image of a linear silicon FZP (the region exposed to the SR beam is framed).

Focusing was carried out in the vertical ( $x, z$ ) plane. The chip was installed on a five-circle goniometer for spatial and angular NCRL positioning when tuning the optical scheme. The focused-beam parameters were estimated using the on-line-program [15]. The experiment was performed using an NCRL with a length  $L = 1.35$  cm (132 elements), for which the strong-absorption condition is fulfilled; i.e., the focused SR beam can be considered as Gaussian with a high accuracy. For the aforementioned parameters of the experiment and NCRL elements, the theoretical values of the focal length and beam size in the focus were  $z_f = 1.11$  cm and  $w_f = 50$  nm, which provided a relatively high angular beam divergence after the focus:  $\Delta\theta = 606$   $\mu$ rad.

As a model sample, we used a linear silicon FZP (Fig. 2b) [17], which was fabricated on a single-crystal silicon membrane with a total thickness  $H_p = 12$   $\mu$ m and had the following parameters: aperture  $A_p = 387$   $\mu$ m, difference in the thicknesses of even (transparent) and odd (opaque) zones  $h_p = 5$   $\mu$ m, outer zone width  $d_p = 0.4$   $\mu$ m, and number of zones  $N_p = 242$ . The FZP in a special holder frame was installed on piezo drivers (SmarAct), providing positioning with a nanoscale accuracy, and arranged so as to make linear zones be oriented perpendicular to the focusing plane and the optical axis  $z$  pass through the transparent zone with the number  $l = 162$ . The width of the FZP zones in this region is  $\sim 0.49$   $\mu$ m. The distances from the NCRL focus to FZP was set to be  $z_0 = 0.75$  cm, which provided illumination of about 10 neighboring zones by the divergent SR beam within the beam FWHM  $w_0 = 4.55$   $\mu$ m. The area of FZP illumination by the SR beam is framed in Fig. 2b.

Intensity distribution images were recorded using a two-dimensional X-ray sCMOS detector XSight

Micron (Rigaku) with a resolution of  $\sim 0.5$   $\mu$ m. The detector was installed at a distance  $z_1 = 19.6$  cm from the sample. Thus, the total length of the experimental scheme (from the NCRL end to the detector) was less than 22 cm at a magnification factor  $M = 27$ . With allowance for the increase in sizes on the detector in comparison with the sample, the effective resolution of the detector in the vertical direction was  $\sim 20$  nm. In the first stage of the experiment, the empty SR beam images after the NCRL focus (without a sample) were recorded in order to estimate the accuracy of tuning the focusing scheme. Then the FZP spatial position after the NCRL focus was tuned, and enlarged phase-contrast images were recorded.

## RESULTS AND DISCUSSION

Enlarged images of the empty SR beam after the NCRL without a sample (on the left) and with a sample (FZP, on the right) are presented in Fig. 3. For one-dimensionally focusing NCRLs, image is magnified in only the vertical direction. For this reason, the scales over the  $x$  and  $y$  axes in the presented images differ by a factor of 10. In theory, when radiation propagates from a point source along the optical axis  $z$  through objects having a constant thickness along the  $y$  axis, the intensity distribution is also independent of  $y$ . The experimentally observed smooth falloff of intensity along the  $y$  axis at the image edges is explained by the finite NCRL aperture along the  $y$  axis and relatively large size of the SR source in the horizontal plane. At the same time, the beam after the NCRL (Fig. 3a) has a Gaussian shape along the  $x$  axis, which corresponds to the theory of focusing using strongly absorbing NCRLs.

A comparison of the images in Fig. 3 shows that the insertion of the FZP into the beam leads to the occur-

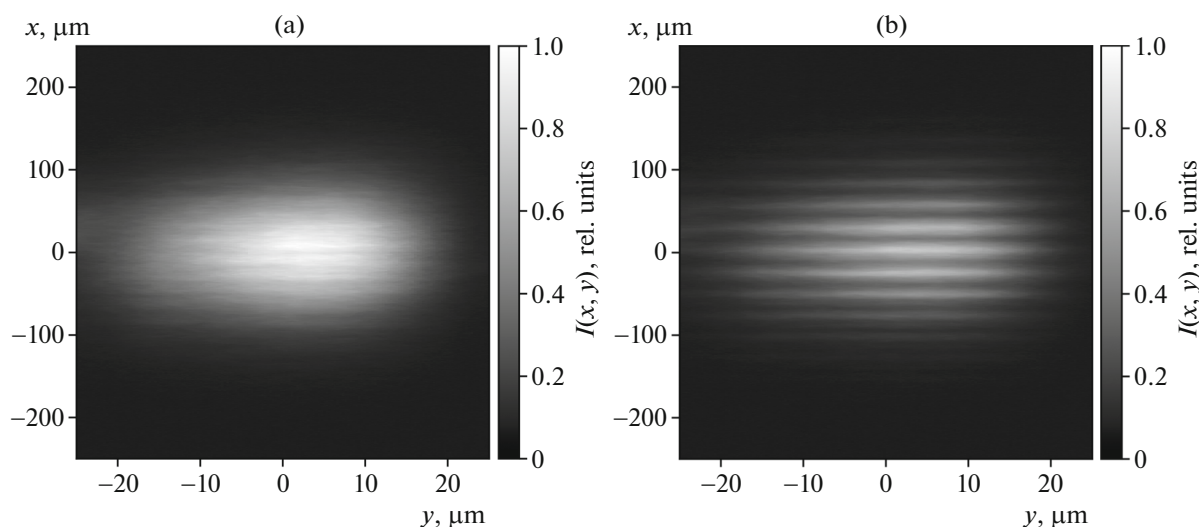


Fig. 3. Experimental images of (a) the SR beam after the NCRL and (b) the FZP phase contrast.

rence of a fairly strong contrast in the intensity distribution (Fig. 3b). The occurrence of the contrast is due to the difference in the SR wave function phases after the FZP in the regions corresponding to zones of different thickness (transparent and opaque zones). It is known that, in the near field for homogeneous objects, contrast is observed primarily at their boundaries, i.e., in the regions of thickness variation. Thus, two intensity peaks and two intensity dips, corresponding to the boundaries of the zone with a sharply changing thickness, should be observed in the image of the FZP structure in near field for each zone. However, the experimental data were obtained for the effective distance  $z_e = 0.73$  cm, at which the near-field condition is not fulfilled strictly for a zone width of  $0.49$   $\mu\text{m}$ . As a result, the contrast at the zone boundaries is blurred, and the experimentally observed intensity peaks and dips correspond, respectively, to the transparent and opaque FZP zones. This effect was considered in [4] when simulating the phase contrast of a photonic crystal. Nevertheless, even in this case the structure period can be experimentally determined with a high accuracy. For example, the distance between the central peaks in the enlarged FZP image is  $26.5 \pm 0.5$   $\mu\text{m}$ . Dividing this value by the magnification factor  $M = 27$ , we obtain  $0.98 \pm 0.02$   $\mu\text{m}$ , which coincides (within the error) with the period of FZP zones in the region exposed to the SR beam. Thus, the proposed scheme of phase-contrast microscopy makes it possible to determine the period of micro-object structure with a submicron spatial resolution, without any complex mathematical processing.

A more detailed analysis of the experimental data is presented in Fig. 4 for the central region of images in Fig. 3. The corresponding experimental intensity distribution curves (round symbols) are given in comparison with the simulation results and least-squares

method (LSM) fitting [18]. Fitting of the SR beam intensity after the NCRL (Fig. 4a) was performed using a Gaussian function, in correspondence with the NCRL focusing theory. The theoretical results of LSM fitting are presented by a solid line. It can be seen that the experimental data are described well within this model, except for the artifacts near the peak value.

The presence of such artifacts may be due to both the SR beam inhomogeneity before the NCRL and the insignificant deviation of the topology of the refracting surface of NCRL elements from a parabolic shape. The model curve FWHM is  $123.5 \pm 0.4$   $\mu\text{m}$ , which coincides (within the error) with the results of theoretical calculation for a point source:  $123.4$   $\mu\text{m}$ . The influence of the SR source finite size is weak at a large distance from the NCRL focus [8]. The coincidence of the experimental and calculation data is indicative of high accuracy of optical scheme tuning and possibility of applying theoretical calculation of NCRL focusing in the analysis of FZP phase-contrast data.

To analyze the experimental curve of FZP phase contrast (Fig. 4b), we performed a theoretical calculation of the intensity distribution at the detector position for a point source using the parameters of the experiment and the FZP parameters. This curve is shown in Fig. 4b by a dashed line. It can be seen that the contrast in the theoretical curve is more detailed as compared with the experimental data, because it is completely coherent. Under real experimental conditions one observes blurring of the coherent phase-contrast pattern, which is caused by the finite size of the SR source and some other factors, including vibrations of optical scheme elements.

As practice shows, the effects causing intensity averaging can be taken into account in simulation using convolution of the calculation results for a point

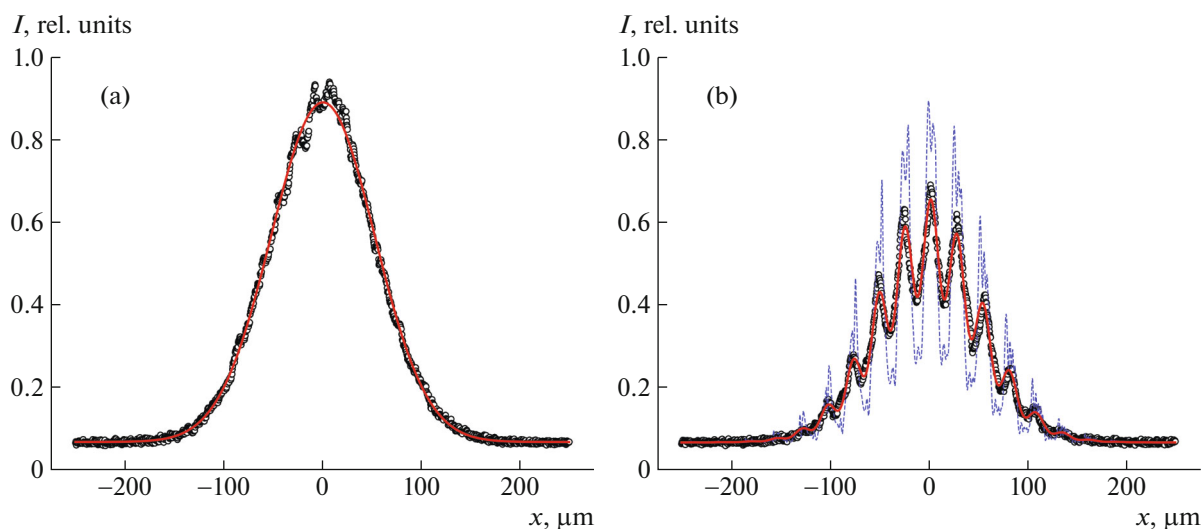


**Fig. 4.** Experimental intensity distribution curves (round symbols) in comparison with the simulation results: (a) SR beam after NCRL and (b) FZP phase contrast. The solid and dashed lines present the LSM simulation results and the results of calculation for a point SR source.

source with the instrumental function in the form of a Gaussian. This procedure is valid for a set of random factors, described by a normal distribution, in view of the associativity of the convolution operation. In simulation the instrumental function FWHM is a variable parameter when the discrepancy between the calculation and experimental curves is minimized by the LSM. The smoothed calculation curve after minimization is shown in Fig. 4b by a solid line. The instrumental function FWHM for the presented curve is  $w_i = 14.4 \pm 0.5 \mu\text{m}$ . It can be seen that, after averaging, the model intensity profile describes fairly exactly the experimental data, which validates the smoothing procedure in use.

The obtained  $w_i$  value determines the spatial resolution of the enlarged phase-contrast image at the detector position. With allowance for the geometric magnification, the effective resolution is determined as  $w_e = w_i/M = 530 \pm 20 \text{ nm}$ . The parameter  $w_e$  may be identified with the enlarged (because of the instrumental function) size of the secondary source in the NCRL focus. The physical meaning of this parameter is as follows: the beam FWHM in the NCRL focus,  $w_f = 50 \text{ nm}$  for a point source, increases due to the finite size of the SR source and displacement of the focus position relative to the sample in the direction perpendicular to the optical axis because of the vibrations.

A calculation of the beam FWHM in the focus with allowance for the vertical size of the SR source ( $100 \mu\text{m}$ ) gives a value of  $132 \text{ nm}$ , which exceeds the value for the point source; however, it is smaller than the experimental value  $w_e$  by a factor of more than 4. Thus, one can suggest that the largest contribution to the deterioration of spatial resolution in the performed

experiment is made by specifically the vibrations of the experimental scheme elements. Having excluded this factor, one can theoretically obtain a resolution as high as  $\sim 100 \text{ nm}$  using the proposed scheme. Even better resolution can be obtained using a coherent SR beam on third- and fourth-generation SR sources.

It is of interest to compare the obtained results with the data of [19] by measuring the SR beam size in the NCRL focus. In this study, we also performed measurements on the XCPM beamline of the KISI-Kurchatov synchrotrone source under similar experimental conditions: radiation energy  $E = 18.6 \text{ keV}$  and NCRL length  $L = 1.1 \text{ cm}$  (104 elements). The theoretical beam FWHM in the focus for these parameters, with allowance for the SR source size, was  $166 \text{ nm}$ . The beam FWHM in the focus was determined by the knife-edge scanning method to be  $460 \pm 70 \text{ nm}$ . The increase in the experimental value in comparison with the theoretical estimate was also explained by the vibrations of optical scheme elements. The beam size in the focus, measured in [19], coincides within the error with the  $w_e$  value obtained here. Thus, the scheme proposed in this study can be used not only to analyze the structure of micro-objects but also to estimate the enlarged (because of the instrumental function) beam size in the NCRL focus using model objects with a known structure. As compared with the knife-edge scanning method, this scheme is simpler, because it does not require to perform many beam scanings in the vicinity of the focus.

## CONCLUSIONS

A new scheme of phase-contrast microscopy based on a silicon NCRL, which is used to form a secondary

SR source, was experimentally implemented for the first time on the XCPM beamline of the KISI-Kurchatov synchrotrone source. A submicron spatial resolution was demonstrated by the example of imaging the structure of the FZP outer zones. The experimental value of the FZP zone period turned out to be  $0.98 \pm 0.02 \mu\text{m}$ , which corresponds to the real period in the region of the FZP illumination by the SR beam. A comparison of the phase-contrast model curves with the experimental data showed that the deterioration of the spatial resolution on the XCPM beamline of the KISI-Kurchatov source is mainly caused by the vibrations of optical scheme elements rather than partial spatial coherence of the SR beam. With this factor excluded and a coherent SR beam used, the scheme proposed in this study theoretically makes it possible to visualize the structure of micro-objects with a resolution below 100 nm. This scheme can also be used to measure the beam size in the NCRL focus, enlarged in comparison with the theoretical value because of the instrumental function influence.

#### FUNDING

The work was carried out within the State assignment of NRC “Kurchatov institute” in the experimental part and the Convention with the Ministry of Science and Higher Education of the Russian Federation on June 28, 2024, no. 075-15-2024-637, in the part concerning the processing and analysis of the results. The work by the V.A. Yunkin on the fabrication of silicon refracting lenses was supported in part by the State assignment no. 075-00296-24-01.

#### CONFLICT OF INTEREST

The authors of this work declare that they have no conflicts of interest.

#### REFERENCES

1. M. V. Koval'chuk, A. E. Blagov, O. S. Naraikin, et al., *Crystallogr. Rep.* **67** (5), 678 (2022). <https://doi.org/10.1134/S1063774522050078>
2. P. A. Prosekov, V. L. Nosik, and A. E. Blagov, *Crystallogr. Rep.* **66**, 867 (2021). <https://doi.org/10.1134/S106377452134006X>
3. A. Snigirev, I. Snigireva, V. Kohn, et al., *Rev. Sci. Instrum.* **66** (12), 5486 (1995). <https://doi.org/10.1063/1.1146073>

4. V. G. Kohn, *Crystallogr. Rep.* **67**, 826 (2022). <https://doi.org/10.1134/S106377452206013X>
5. V. Yunkin, M. V. Grigoriev, S. Kuznetsov, et al., *Proc. SPIE* **5539**, 226 (2004). <https://doi.org/10.1117/12.563253>
6. A. Snigirev, I. Snigireva, V. Kohn, et al., *Phys. Rev. Lett.* **103**, 064801 (2009). <https://doi.org/10.1103/PhysRevLett.103.064801>
7. T. S. Argunova and V. G. Kohn, *Usp. Fiz. Nauk* **189** (6), 643 (2019). <https://doi.org/10.3367/UFNr.2018.06.038371>
8. M. S. Folomeshkin, V. G. Kohn, A. Yu. Seregin, et al., *Crystallogr. Rep.* **68** (1), 1 (2023). <https://doi.org/10.1134/S1063774523010078>
9. V. G. Kohn, *JETP Lett.* **76**, 701 (2002). <https://doi.org/10.1134/1.1541043>
10. V. G. Kohn, *J. Exp. Theor. Phys.* **124**, 224 (2003). <https://doi.org/10.1134/1.1600812>
11. V. G. Kohn, *J. Synchrotron Radiat.* **25**, 1634 (2018). <https://doi.org/10.1107/S1600577518012675>
12. V. G. Kohn and M. S. Folomeshkin, *J. Synchrotron Radiat.* **28**, 419 (2021). <https://doi.org/10.1107/S1600577520016495>
13. V. G. Kohn, *J. Synchrotron Radiat.* **29**, 615 (2022). <https://doi.org/10.1107/S1600577522001345>
14. V. G. Kohn (2024). <https://xray-optics.ucoz.ru/XR/xrwp.htm>
15. V. G. Kohn (2024). <https://kohnvict.ucoz.ru/jsp/1-crl-par.htm>
16. V. G. Kohn, P. A. Prosekov, A. Y. Seregin., et al., *Crystallogr. Rep.* **64** (1), 24 (2019). <https://doi.org/10.1134/S1063774519010139>
17. I. Snigireva, A. Snigirev, and V. Kohn, *Phys. Status Solidi A* **204** (8), 2817 (2007). <https://doi.org/10.1002/pssa.200675702>
18. W. Press, S. Teukolsky, W. Vetterling, et al., *Numerical Recipes, The Art of Scientific Computing* (Cambridge Univ. Press, Cambridge, 2007).
19. M. N. Sorokovikov, D. A. Zverev, A. A. Barannikov, et al., *Nanobiotechnol. Rep.* **1**, 1. P. S210 (2023). <https://doi.org/10.1134/S2635167623601183>

*Translated by Yu. Sin'kov*

**Publisher's Note.** Pleiades Publishing remains neutral with regard to jurisdictional claims in published maps and institutional affiliations. AI tools may have been used in the translation or editing of this article.